A screening campaign in sea urchin egg homogenate as a platform for discovering modulators of NAADP-dependent Ca^{2+} signaling in human cells

Gihan S. Gunaratne[a], Malcolm E. Johns[a], Hallie M. Hintz[a], Timothy F. Walseth[a], Jonathan S. Marchant[b],*

[a] Department of Pharmacology, University of Minnesota Medical School, MN 55455, USA
[b] Department of Cell Biology, Neurobiology and Anatomy, Medical College of Wisconsin, Milwaukee WI 53226, USA

ABSTRACT

The Ca^{2+} mobilizing second messenger nicotinic acid adenine dinucleotide phosphate (NAADP) regulates intracellular trafficking events, including translocation of certain enveloped viruses through the endolysosomal system. Targeting NAADP-evoked Ca^{2+} signaling may therefore be an effective strategy for discovering novel antivirals as well as therapeutics for other disorders. To aid discovery of novel scaffolds that modulate NAADP-evoked Ca^{2+} signaling in human cells, we have investigated the potential of using the sea urchin egg homogenate system for a screening campaign. Known pharmacological inhibitors of NAADP-evoked Ca^{2+} release (but not cADPR- or IP$_3$-evoked Ca^{2+} release) in this invertebrate system strongly correlated with inhibition of MERS-pseudovirus infectivity in a human cell line. A primary screen of 1534 compounds yielded eighteen 'hits' exhibiting > 80% inhibition of NAADP-evoked Ca^{2+} release. A validation pipeline for these candidates yielded seven drugs that inhibited NAADP-evoked Ca^{2+} release without depleting acidic Ca^{2+} stores in a human cell line. These candidates displayed a similar penetrance of inhibition in both the sea urchin system and the human cell line, and the extent of inhibition of NAADP-evoked Ca^{2+} signals correlated well with observed inhibition of infectivity of a Middle East Respiratory syndrome coronavirus (MERS-CoV) pseudovirus. These experiments support the potential of this simple, homogenate system for screening campaigns to discover modulators of NAADP, cADPR and IP$_3$-dependent Ca^{2+} signaling with potential therapeutic value.

1. Introduction

Ca^{2+} signals originating from the 'acidic' Ca^{2+} stores of endosomes and lysosomes regulate a steadily growing list of cellular and developmental processes [1]. One important endolysosomal Ca^{2+} release pathway is activated by nicotinic acid adenine dinucleotide phosphate (NAADP), a potent Ca^{2+} releasing second messenger in many cells and tissues [1–3]. NAADP mobilizes intracellular Ca^{2+} stores by engaging the activity of members of the two-pore channel (TPC) family ([4–9], but see [10,11]). TPCs are broadly expressed ion channels and evolutionarily ancient members of the voltage-gated ion channel superfamily [12,13]. Their identification and subsequent study has facilitated resolution of many pathophysiology processes dependent upon endolysosomal Ca^{2+} release [14–16]. For example, using knockdown or knockout approaches, a role for TPCs has been shown during viral infectivity [17], Parkinson disease [18], muscle function and development [11,19–21], late-onset obesity [22] and susceptibility to non-alcoholic fatty liver disease [23]. Such discoveries prioritize the importance of identifying small molecule

modulators of TPC- and NAADP-dependent Ca^{2+} signaling pathways as research tools and perhaps, over the longer term, as a therapeutic avenue. For example, the natural product tetrandrine recently identified as a TPC blocker and inhibitor of NAADP-evoked Ca^{2+} signaling improved survival in mice infected with Ebola [17]. Modulators of NAADP-dependent signaling have been shown to be effective against other eukaryotic pathogens [24] and viral infections [17,25] as well as regulators of neoangiogenesis [26,27].

Current pharmacological tools for inhibiting NAADP-evoked Ca^{2+} signals comprise several groups. First, compounds that generally perturb the mobilizable, organellar Ca^{2+} pool (e.g. bafilomycin, a vacuolar H$^+$-ATPase inhibitor and various lysosomal disruption agents [28,29]). Second, agents that interfere with NAADP binding, including *trans*-Ned-19 (a member of a NAADP conformer series identified by virtual screening, [30]) and the nucleotide mimetics PPADS and PPNDS [31]. Third, agents that act as TPC pore blockers, including Ca$_v$ channel antagonists (diltiazem, nifedipine, < 10 u M [13,32]) and possibly tetrandrine (sub-micromolar range [17] and structurally-related

derivatives [25]. Finally, a flotilla of other compounds working through the above mechanisms that have inhibitory actions over a range of tens of micromolar. These include alkyl pyridinium analogs (IC$_{50}$ ~15μM, [33]) Na$_v$ blockers (IC$_{50}$ > 100μM, [13]) and naringenin (IC$_{50}$ ~180μM, [27]). Overall, there is scope for identifying an improved pharmacopeia of selective, potent modulators of the NAADP-evoked Ca^{2+} release pathway.

One approach for executing an unbiased screening campaign targeting NAADP-sensitive Ca^{2+} signaling is based upon interrogation of Ca^{2+} release responses in the sea urchin egg homogenate system, the preparation in which the Ca^{2+} releasing activity of NAADP (and cyclic ADP ribose, cADPR) was first discovered [34,35]. The sea urchin egg homogenate system represents a simple, yet robust preparation [36]: it is an easily prepared cell-free system that, within each independent preparation, provides reproducible and robust responsiveness to multiple Ca^{2+}-releasing second messengers (NAADP, cADPR and IP$_3$) within a minaturizable, high signal-to-noise, room temperature assay. Homogenate can be prepared in bulk, and stored as frozen aliquots which remain responsive for many years. For all these reasons, the system has long been regarded as the 'gold-standard' for studying NAADP action [34,35], and has been frequently used to assess the action of molecules eliciting Ca^{2+} release through each of the discrete, endogenous Ca^{2+} mobilization pathways [13,30,32,33,37–42]. Although the system is clearly amenable to high throughput profiling, no screening campaign has, to our knowledge, yet been reported. This is surprising given the many advantages of this preparation, not in the least the intrinsic sensitivity to the three Ca^{2+}-releasing second messengers that permits counter-screening of small molecule specificity. Here, we have performed a pilot screen for novel modulators of NAADP-sensitive Ca^{2+} release in the sea urchin egg homogenate system and assessed tractability of the resulting 'hits' against both endogenous NAADP-evoked Ca^{2+} responses and a pseudotyped MERS-CoV translocation assay in human cell lines [25].

2. Materials & methods

2.1. Drugs and molecular reagents

Chemicals were sourced as follows: fluo-4 AM and LysoTracker Red (LTR, Thermo Scientific); fluo-3 pentapotassium salt (Biotium). Gly-Phe-β-naphthylamide (GPN, Santa Cruz Biotechnology); PF-543, SKF 96365 hydrochloride, LY-310,762 hydrochloride, PDMP hydrochloride, and PPADS tetrasodium salt (Cayman Chemical); fluphenazine dihydrochloride, GBR-12935 dihydrochloride, racecadotril, clemastine fumarate, prochlorperazine dimaleate salt, thioridazine hydrochloride, salmeterol xinafoate, oxybutynin chloride, trifluoperazine dihydrochloride, naringenin, HEPES, CHAPS, potassium gluconate, N-methylglucamine, NAD, NAAD, NADP, nicotinamide mononucleotide, nicotinic acid, nicotinamide, ATP, and DTT (Sigma Aldrich); A-315456, 3-(1H-Imidazol-4-yl)propyl di(p-fluorophenyl)methyl ether hydrochloride (IPFME), ST-148, TMB-8 hydrochloride, and trans-Ned-19 (Santa Cruz Biotechnology); dilazep hydrochloride (Tocris); cOmplete™ EDTA-free protease inhibitor cocktail (Roche). NAADP and cADPR were synthesized in house using previously described methods [40,43]. The libraries used for screening activities were sourced from Sigma (LOPAC$^{®1280}$, Library of Pharmacologically Active Compounds, 1280 compounds) and Selleck (GPCR compound library, 254 compounds). For the LOPAC$^{®1280}$ library all compounds were screened in triplicate (n = 3, independent assays). For the smaller GPCR library, compounds were screened in duplicate (n = 2, independent assays), owing to limitations on material.

2.2. Ca^{2+} release assays in sea urchin egg homogenate

Strongylocentrotus purpuratus homogenates (25%) were prepared as previously described [44] and stored at −80 °C for subsequent usage.

Homogenates were loaded with Ca^{2+} and fluo-3 by incubation at 17 °C in an intracellular medium, consisting of 250 mM potassium gluconate, 250 mM N-methyl-D-glucamine, 20 mM HEPES, 1 mM MgCl$_2$, pH 7.2, supplemented with 0.3 mg/mL creatine kinase, 0.5 mM ATP, 4 mM phosphocreatine, and 3μM Fluo-3 [45]. Homogenate was diluted in a step-wise fashion over the course of 3 h to a final concentration of 1.25% homogenate. Fluo-3 fluorescence was monitored using a Tecan Infinite M1000 Pro plate reader (λ_{ex} = 485 ± 5 nm, λ_{em} = 525 ± 5 nm). Baseline fluorescence readings from samples in the presence of individual drugs were measured, followed by stimulation with a submaximal concentration of NAADP.

2.3. Screening protocols

The screening studies were performed in 96-well assay plates (Corning 3590 flat bottom, transparent) and each library was screened at a final concentration of 25μM. An epMotion® 96 liquid handling workstation (Eppendorf) was used to dispense homogenate and NAADP into assay plates. Fluo-3 fluorescence was monitored using a Tecan Infinite M1000 Pro plate reader. For all screening experiments, fluo-3 fluorescence changes were monitored in the presence of compound for 35 cycles (6 min) prior to the addition of an EC$_{90}$ concentration of NAADP (167 nM final concentration). For the LOPAC$^{®1280}$ library, 0.25ul of vehicle (DMSO) or compound (10 mM) was dispensed into the assay plates using a LabCyte ECH0550 acoustic nanoliter dispensing system. The assay was started by addition of 99.75 μl of sea urchin egg homogenate. For experiments screening the Selleck GPCR compound library, baseline fluo-3 fluorescence of the homogenate (97.5ul) was monitored for 1.5 min prior to the addition of 2.5ul vehicle (DMSO) or compound (1 mM) using the epMotion® 96. Z' values were calculated to assess separation of distributions of positive and negative controls, as described elsewhere [45].

2.4. ^{32}P-NAADP binding and Ca^{2+} release assays in sea urchin egg homogenate

[^{32}P]-NAADP was synthesized from [^{32}P]-NAD and used for binding studies as previously described [45,46].

2.4.1. Mammalian cell line imaging

For imaging experiments to assess changes in lysosome properties and Ca^{2+} content, human U2OS cells (bone osteosarcoma) were seeded in optical bottom black walled 96-well plates (Thermo Scientific) at a density of 6 × 10^5 cells per well. After 4 h at 37 °C and 5% CO$_2$, cells were loaded with LysoTracker® Red (LTR) and fluo-4 AM according to the vendors' respective protocols. Cells were then thoroughly rinsed and media was replaced with Hanks Balanced Salt Solution (HBSS, Thermo Scientific). Fluorescence of LTR (λ_{ex} = 575 ± 5 nm, λ_{em} = 590 ± 5 nm) and fluo-4 (λ_{ex} = 490 ± 5 nm, λ_{em} = 506 ± 5 nm) were simultaneously monitored using a Tecan Infinite M1000 Pro plate reader at 37 °C. Baseline fluorescence values were monitored for 10 cycles, followed by addition of either vehicle or drug (final concentration, 30μM) and changes in fluorescence values were monitored for an additional 35 cycles. Cells were then treated with GPN (final concentration, 300μM) to stimulate osmotic disruption of lysosomes and Ca^{2+} release with fluorescence monitored for a further 35 cycles. Changes in lysosomal Ca^{2+} content due to drug treatment were quantified by assessing fluorescence ratios (F/F$_0$) during GPN treatment in control and drug-treated samples, where 'F' represents fluo-4 fluorescence at peak, and F$_0$ represents fluorescence at time = 0. Changes in lysosomal labelling due to drug treatment were quantified by assessing fluorescence ratios (F/F$_0$) of LTR during drug treatment, where again 'F' represents minimum LTR fluorescence ratio after drug addition prior to GPN treatment, and 'F$_0$' represents LTR fluorescence at time = 0. NAADP microinjection assays in human U2OS cells were performed as described in the companion paper [25].

2.5. Cell viability assays

U2OS cells were seeded in white 96-well plates (Corning) at a density of 2×10^5 cells per well. The following day, cell cultures were supplemented with test compounds or vehicle for 8 h at 37 °C and 5% CO_2. Viability of the cells was assessed using CellTiter-Glo 2.0 (Promega) according to the vendor's protocol. ATP-dependent luciferase activity from CellTiter-Glo 2.0 reagent was quantified using a plate reader (Tecan Infinite M1000 Pro).

2.6. MERS-CoV translocation assay

MERS pseudovirus experiments were performed in Huh7 cells (human hepatocyte-derived carcinoma) as described in the companion paper [25]. In brief, MERS-CoV spike pseudotyped retroviruses expressing a luciferase-encoding reporter gene was generated by transfecting HEK293 T cells with plasmid carrying Env-defective, luciferase-expressing HIV-1 genome (pNL4-3.luc.RE) and plasmid encoding MERS-CoV Spike protein. Following receptor-mediated endocytosis of the MERS-pseudovirus, translocation of the viral particle from the lumen of the endolysosomal system to the cytosplasm is detected 72 h post infection by measuring luciferase activity.

3. Results

As an initial feasibility test for the validity of screening sea urchin egg homogenate to discover leads with mammalian activities, we took advantage of our existing compound dataset resulting from the MERS pseudovirus bioassay [25]. A set of compounds, known to display various degrees of attenuation of MERS pseudovirus infectivity, were screened for inhibition of Ca^{2+} release in the sea urchin egg homogenate system. A typical experiment is shown in Fig. 1A, which resolves Ca^{2+} release kinetics evoked by NAADP, or cADPR or IP$_3$ in the absence and presence of fangchinoline. Fangchinoline, an inhibitor of NAADP-evoked Ca^{2+} signals and MERS pseudovirus translocation in a human cell line [25], decreased the magnitude of NAADP-evoked Ca^{2+} release

(peak amplitude 47 ± 2% of control response, blue traces in Fig. 1A) with lesser effects on the size of IP$_3$ or cADPR-evoked Ca^{2+} transients (Fig. 1A). Ca^{2+} release assays were performed for ~20 other ligands shown to be inhibitors in the MERS pseudovirus translocation assay, and then the impact of these ligands on Ca^{2+} signals evoked by NAADP-, cADPR- and IP$_3$ were correlated with effects in the viral assay (Fig. 1B). Inspection of regression plots from each dataset revealed that compounds that inhibited NAADP-evoked Ca^{2+} release were associated with blockade of MERS pseudovirus translocation, with more effective NAADP inhibitors causing greater decreases in infectivity (Fig. 1B). No positive correlation was seen for the identical set of compounds between modulation of either cADPR or IP$_3$-evoked signals and MERS pseudovirus translocation (Fig. 1B). Overall, these data establish that identification of pharmacological inhibitors of NAADP-evoked Ca^{2+} signals in the sea urchin system has potential utility for discovering modulators of NAADP dependent processes in human cells, such as MERS pseudovirus translocation [25]. This provides rationale for a broader screening campaign against sea urchin egg homogenate to discover novel modulators of NAADP-evoked Ca^{2+} release.

3.1. Screening sea urchin egg homogenate for novel inhibitors of NAADP-evoked Ca^{2+} release

A schematic overview of the four-step screening workflow is shown in Fig. 2A. The primary screen (fixed concentration of 25μM, 1534 compounds), and secondary validation of potential 'hits' (full concentration response curve analysis), were both performed using sea urchin egg homogenate (steps '1' and '2') in a miniaturized format (96-well plate). These activities would be predicted to yield a smaller number of candidates for the subsequent, more laborious validation approaches in a human cell line (U2OS). These final activities (steps '3' and '4') encompassed: (i) counter-screening for more generalized actions against acidic Ca^{2+} stores, for example lysosomotropism [28,29], (ii) quantifying effects on NAADP-evoked Ca^{2+} signals evoked by single cell microinjection of NAADP, and (iii) correlating effects on Ca^{2+} release with bioactivities in the MERS pseudovirus translocation assay.
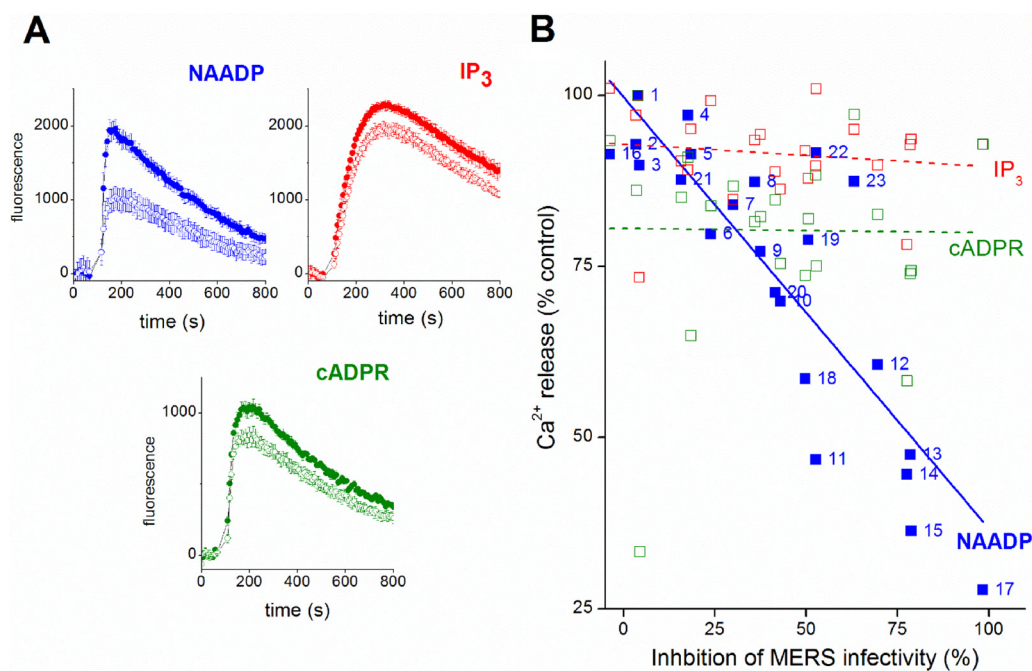
Fig. 1. Drugs that inhibit NAADP-evoked Ca^{2+} release block MERS translocation. **A**, Ca^{2+} release in sea urchin egg homogenate as resolved by fluo-3 fluorescence measurements. Ca^{2+} liberation was measured in the absence (solid circles, top trace) or presence of fangchinoline (open circles, 10μM) in response to NAADP (blue, 70 nM), IP$_3$ (red, 200 nM) or cADPR (green, 100 nM). Data represent values from a minimum of three independent experiments and are expressed as mean ± SEM. **B**, correlation plot comparing the extent of inhibition of NAADP- (blue) IP$_3$- (red) or cADPR-evoked Ca^{2+} release (green) observed with individual ligands (10μM) correlated with the extent of inhibition of MERS-pseudovirus translocation evoked by the same ligands (at the same concentration, 10μM). None of these tested ligands evoked Ca^{2+} release by themselves. Solid (NAADP) and dotted lines (IP$_3$, cADPR) represent linear regression of datapoints. Ligand key: 1 = DMSO, 2 = Cycleanine, 3 = Tubocurarine, 4 = Nimodipine, 5 = Procaine, 6 = Chondocurine, 7 = Benzocaine, 8 = Hernandezine, 9 = Berbamine, 10 = Nicardipine, 11 = Verapamil, 12 = Tetrandrine, 13 = Fangchinoline, 14 = Amitriptyline, 15 = Loperamide, 16 = Ned-19, 17 = Bafilomycin, 18 = U18666 A, 19 = YM201636, 20 = Fluoxetine, 21 = Citalopram, 22 = Desipramine, 23 = Siramesine. MERS-pseudovirus infectivity was measured using a luciferase-based cell entry assay, assay methodology and inhibition of NAADP-evoked Ca^{2+} shown in this figure are described in detail in the companion paper [25].

A

step

① 1° screen   *urchin*

25μM, 1534 cmpds

→

② 2° screen   *urchin*

IC$_{50}$ Ca^{2+} release
selectivity
binding

→

③ counterscreen   *mammalian*

acidic Ca^{2+} pools

→

④ validation   *mammalian*

NAADP-evoked
Ca^{2+} release

MERS translocation
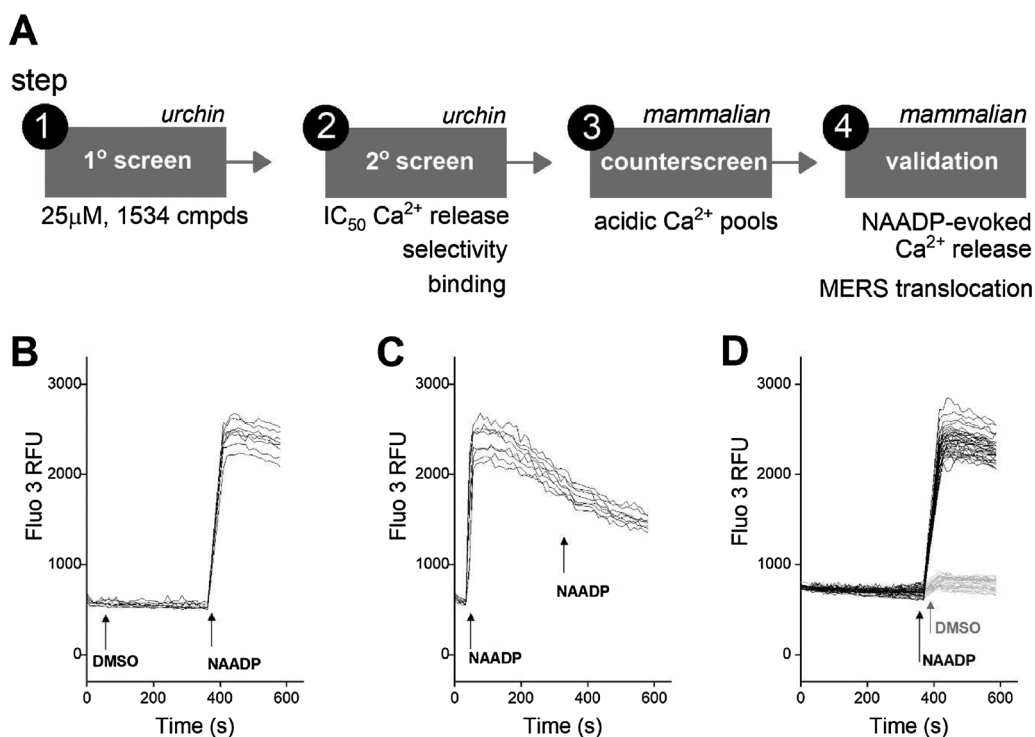
Fig. 2. Schematic of workflow for identification of inhibitors of NAADP-evoked Ca^{2+} release and screening assay validation. **A,** Illustration of screening workflow. Small molecule libraries (1534 compounds) were screened for inhibitors of NAADP-evoked Ca^{2+} release in sea urchin egg homogenate. Primary screen hits were validated and characterized prior to testing against Ca^{2+} signals evoked by NAADP microinjection and pseudo-typed MERS-CoV cell entry in mammalian cells. **B,** Representative traces of fluo-3 fluorescence for negative control in response to addition of vehicle (1st injection) and then NAADP (2nd injection, 167 nM) at indicated timepoints (arrows). **C,** Representative traces showing example of positive control (initial injection with NAADP, 167 nM). **D**, Representative traces of fluo-3 fluorescence used to measure Z' after the 2nd injection timepoint (arrows).

The overall pipeline would therefore evaluate the translatability of compounds discovered from urchin screening platform for modulating NAADP-evoked Ca^{2+} signaling in mammalian cells.

First, we optimized conditions for executing the miniaturized screen in sea urchin egg homogenate, defining a basic protocol depicted in Fig. 2B. Compounds were preincubated with homogenate for 6 min (1st addition) during which fluorescence readings were monitored, followed by a single subsequent addition of NAADP (167 nM, 2nd addition). The positive control was NAADP itself (1st addition, Fig. 2C), known to self-desensitize the sea urchin NAADP-evoked Ca^{2+} release pathway [46]. The negative control was dual additions of vehicle (Fig. 2D). These positive (NAADP) and negative vehicle (DMSO) controls were run in parallel for each plate. The robustness of the screening platform was assessed by calculating the Z' factor (Z'), a widely employed indicator of assay quality in screening applications [47]. Z' values over 0.5 are considered a prerequisite for executing reliable higher throughput screens. Calculations of Z' were therefore made using peak fluorescence values during the NAADP-evoked Ca^{2+} mobilization response after initial preincubation with vehicle control versus dual vehicle additions (Fig. 2D), averaging 8 replicate wells within a 96 well plate. Using this protocol, Z' = 0.73 ± 0.12, an acceptable value defining assay conditions for subsequent experiments.

The primary screen (1534 compounds) was then performed using two libraries (LOPAC®1280, 1280 compounds; and a G protein coupled receptor (GPCR) library, 254 compounds). Results of the dual library screens are presented together in Fig. 3A which collates the averaged magnitude of the NAADP-evoked Ca^{2+} signal observed following preincubation with each compound. These data were then replotted (Fig. 3B) as a progressive ranking of inhibition from the most penetrant inhibitor (PF-543) through to compounds that showed potentiation versus the control NAADP signal (phenytoin). Most compounds (~87% of those screened) fell within a ± 25% range of control values (shaded area, Fig. 3B). Reassuringly, two established inhibitors of NAADP-evoked Ca^{2+} release and ^{32}P-NAADP binding in the sea urchin egg homogenate system – the purinergic blockers PPADS and PPNDS [31] – displayed clear inhibitory effects in the primary screen, with NAADP-evoked Ca^{2+} release reduced to 40 ± 8% (PPADS) and 22 ± 4% (PPNDS) of control values (Fig. 3C).

As our focus here was on identifying novel, penetrant inhibitors of NAADP signaling, an arbitrary cut-off of > 80% inhibition of the control NAADP-evoked Ca^{2+} signal amplitude was used for candidate prioritization (red box, Fig. 3D), a threshold which corralled 20 compounds. Compounds that caused changes or elevations of baseline fluorescence values during the preincubation period were also excluded from subsequent analysis, one example being the ionophore A23187 (Fig. 3). Another example was the SERCA inhibitor thapsigargin, which depleted the ER Ca^{2+} content, but did not abrogate NAADP responsiveness from the acidic Ca^{2+} stores (Fig. 3C). Also excluded were known modulators of NAADP-evoked Ca^{2+} signaling such as thio-NADP (known to contain contaminating NAADP [48], Fig. 3C). Following this pruning, a top cohort of 18 putative inhibitors was prioritized and ranked (#1, PF-543 through #18, trifluoperazine; Fig. 3D). Analysis of the known pharmacological activities of the screened ligands, and comparison with the subset of these top eighteen candidate inhibitors, revealed enrichment of the 'neurotransmission' classification and dopaminergic modulators in particular (Supplementary Fig. 1). Table 1 collates the ranking of these 18 candidate hits from the primary screen and subsequent data from other assays in the screening pipeline.

Three compounds showed > 90% inhibition of NAADP-evoked Ca^{2+} signaling in the primary screen (Fig. 3E). The top two hits were PF-543 (rank #1, 6.0 ± 5.0% of control NAADP response) and SKF96365 (rank #2, 6.3 ± 4.5% of control NAADP response). PF-543 is a cell permeable inhibitor of sphingosine kinase 1 (K$_i$ ~ 4 nM, [49]), which catalyzes the formation of sphingosine 1-phosphate from sphingosine; SKF96365 is a LVA T-type Ca$_v$ blocker, with additional antagonist action at TRPC channels and other Ca$_v$s [50,51].

Secondary validation of the primary screening hits was then performed (step '2', Fig. 2). For each of the top hits, full concentration response curves for inhibition of NAADP-evoked Ca^{2+} release in the sea urchin egg homogenate was performed. Representative curves are shown in Fig. 4A, and IC$_{50}$ values for each compound are collated in Table 1. Each of the eighteen prioritized candidates elicited a concentration-dependent inhibition of NAADP-evoked Ca^{2+} release, validating the robustness of the primary screen. IC$_{50}$ values spanned from low micromolar (e.g. racecadotril, IC$_{50}$ = 1.6 ± 0.1μM) to tens of micromolar, a range that compares favorably with data obtained with
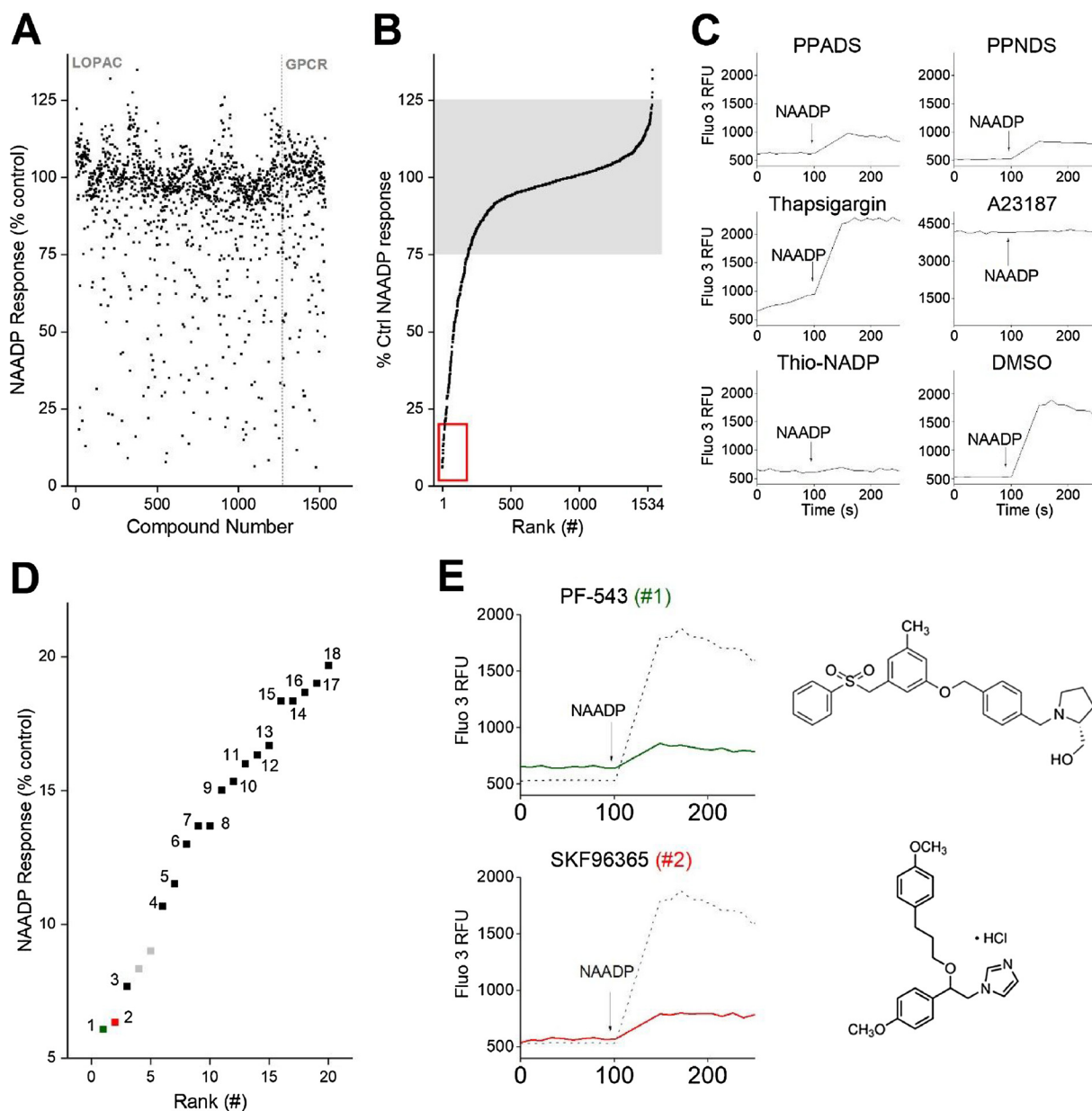
Fig. 3. Identification of top hits from primary drug screen. **A,** Scatter plot of average peak amplitude of NAADP-evoked Ca^{2+} release in the presence of drug (25μM) from LOPAC*1280 (left, numbered 1–1280) or Selleck (GPCR) compound library (right, numbered 1281–1534). **B,** results from both libraries were combined and compounds were ranked by amplitude of response from greatest inhibition (rank #1, left) to potentiation (rank #1534, right). The majority of compounds were in a range ± 25% of control response (shaded box). Compounds that exhibited > 80% inhibition of NAADP-evoked Ca^{2+} release were prioritized (red box) and selected for further characterization (Table 1). **C,** raw data from the primary screen for selected compounds – PPADS, PPNDS, thapsigargin, A23187, thio-NADP and vehicle control (DMSO). **D,** enlargement of red box from 'B' showing ranking of top eighteen hits after pruning, which displayed > 80% inhibition of NAADP-evoked Ca^{2+} release. Pruned compounds were thio-NADP and A23187 (4th and 5th top hits), shown in grey. **E,** traces of NAADP-evoked Ca^{2+} release in the presence of the two top ranked candidates (#1, PF-543; #2, SKF96365; coloured lines, 25μM).

currently used inhibitors of NAADP evoked Ca^{2+} signals, including PPADS (IC_{50} = 5.4 ± 0.2μM) and the lower potency of commercially sourced *trans*-ned-19 in our hands (156 ± 3μM, but compare with [30]). A recently proposed TPC2 inhibitor - naringenin [27] – also displayed little inhibitory activity in this system. The selectivity of inhibition of the NAADP pathway was assessed by monitoring effects of the same candidate (30μM) on IP_3-evoked Ca^{2+} signals, cADPR-evoked Ca^{2+} signals and NAADP-evoked Ca^{2+} signals. Representative compounds in this assay are shown in Fig. 4B. Finally, the effects of compound on ^{32}P-NAADP binding was also examined, as one potential mechanism for inhibition of NAADP-evoked Ca^{2+} responses. Except for NAADP and the positive control PPADS, none of the compounds

displayed significant inhibition of ^{32}P-NAADP binding in sea urchin egg homogenates (Fig. 4C). These data were also consistent with a failure of the candidates to displace a photoaffinity probe [8,45,52–54] from the NAADP receptor binding protein in mammalian U2OS cell extracts (data not shown).

3.2. Counterscreening in mammalian cells

These sea urchin screening activities generated a group of eighteen compounds that merited assessment for activities against NAADP-evoked Ca^{2+} signaling in human cells (steps '3' and '4', Fig. 2A). To generate a priority order for assessing inhibition of responses to

Table 1

Summary of compounds from primary screen with > 80% inhibition of NAADP-evoked Ca^{2+} release. Compounds were ranked (#1 through #18) in order of maximum average inhibition of NAADP-evoked Ca^{2+} release in the primary screen (Fig. 3). Hits were then further assessed in concentration-response and ^{32}P-NAADP binding experiments in sea urchin egg homogenate (Fig. 4). Counter-screening activities were performed in U2OS cells, with the cut-off threshold for non-pursuit of the candidates being > 30% decrease in fluorescence ratios in either Ca^{2+} release or LTR assays. Validation assays represent extent of inhibition of NAADP-evoked Ca^{2+} release signals, and MERS pseudovirus translocation by the remaining seven candidates (bold in compound list). IPFME (rank #8): 3-(1H-Imidazol-4-yl) propyl di(p-fluorophenyl)methyl ether hydrochloride.

Compound	1 °Screen	2 °Screen		Counterscreen		Validation	
	(sea urchin)	(sea urchin)		(human cells)		(human cells)	
	Ca^{2+} release (% NAADP)	Ca^{2+} release $log(IC_{50})$	NAADP binding (% inhibition)	Ca^{2+} release (% GPN)	LTR signal (% control)	Ca^{2+} release (% NAADP)	MERS (% control)
PF-543	6.0 ± 0.4	−5.44 ± 0.18	5.9 ± 2.2	94.0 ± 4	95.3 ± 3	14.1 ± 3.0	18.8 ± 2.1
SKF 96,365	6.3 ± 4.5	−5.29 ± 0.06	−5.3 ± 5.7	98.1 ± 6	98.5 ± 5	12.4 ± 8.9	22.1 ± 7.8
Fluphenazine dihydrochloride	7.7 ± 8.3	−4.97 ± 0.03	3.2 ± 1.5	67.6 ± 14	69.8 ± 10		
GBR-12935 dihydrochloride	10.7 ± 7.0	−4.90 ± 0.13	3.4 ± 3.3	61.1 ± 15	67.5 ± 11		
Racecadotril	11.5 ± 6.0	−5.80 ± 0.03	−8.3 ± 0.2	110.0 ± 4	92.8 ± 3	16.6 ± 10	20.3 ± 4.1
A-315456	13.0 ± 5.0	−4.44 ± 0.01	8.4 ± 1.2	97.1 ± 3	95.2 ± 4	41.1 ± 14	56.7 ± 9.3
Clemastine fumarate	13.7 ± 15	−4.78 ± 0.09	8.2 ± 3.6	69.5 ± 13	70.9 ± 15		
IPFME	13.7 ± 11	−5.22 ± 0.08	2.9 ± 2.1	51.3 ± 18	56.9 ± 8		
Prochlorperazine dimaleate	15.0 ± 12	−4.62 ± 0.27	0.0 ± 3.4	20.2 ± 17	24.3 ± 14		
Thioridazine hydrochloride	15.3 ± 17	−4.77 ± 0.02	−3.3 ± 1.5	20.5 ± 12	26.2 ± 18		
Dilazep hydrochloride	16.0 ± 3.0	−5.03 ± 0.11	−10.9 ± 8.1	65.1 ± 5	69.6 ± 9		
LY-310,762 hydrochloride	16.3 ± 8.7	−4.75 ± 0.05	−2.8 ± 3.8	108.1 ± 11	90.2 ± 8	42.9 ± 5.1	82.2 ± 5.1
ST-148	16.7 ± 3.5	−4.80 ± 0.08	0.2 ± 4.3	66.6 ± 5	69.8 ± 13		
TMB-8 hydrochloride	18.3 ± 3.2	−5.12 ± 0.06	−16.6 ± 10.3	68.8 ± 5	71.8 ± 8		
PDMP	18.3 ± 17	−4.80 ± 0.05	6.0 ± 0.5	91.4 ± 2	91.6 ± 13	43.7 ± 15	65.4 ± 7.3
Salmeterol xinafolate	18.7 ± 12	−4.94 ± 0.04	−2.3 ± 13.6	97.4 ± 5	97.3 ± 7	26.7 ± 7.2	32.9 ± 4.7
Oxybutynin Chloride	19.0 ± 10	−5.07 ± 0.05	−6.0 ± 5.2	62.1 ± 4	59.2 ± 9		
Trifluoperazine dihydrochloride	19.7 ± 15	−5.13 ± 0.10	−13.7 ± 13.7	5.8 ± 11	15.2 ± 9		
PPADS (positive control)	*40.0 ± 13*	*−5.27 ± 0.01*	*84.8 ± 1.6*	*91.3 ± 16*	*92.1 ± 7*	*24.2 ± 2.1*	*26.0 ± 3.8*
DMSO (negative control)	*94.5 ± 2*	*n/a*	*2.1 ± 4.8*	*93.0 ± 3*	*97.6 ± 2*	*94.5 ± 13*	*97.3 ± 2.1*

microinjected NAADP in single cells, which is a relatively time-consuming process, we first counter-screened the compounds for deleterious effects on cell viability, or non-specific actions on the acidic Ca^{2+} stores. The cell viability screen was performed using a luciferase based system to quantify cellular ATP levels following incubation of U2OS cells (bone osteosarcoma) with each compound. None of the compounds exhibited toxicity over this treatment paradigm compared to control samples (Supplementary Fig. 2).

Next, the effects of the candidate drugs on lysosomal number and Ca^{2+} content were assessed by simultaneously monitoring changes in LysoTracker® fluorescence and cytoplasmic Ca^{2+} following addition of GPN (glycyl-L-phenylalanine-2-naphthylamide). GPN causes lysosomal permeabilization and Ca^{2+} release, concomitant with loss of LysoTracker® staining intensity [55,56]. Decreased lysosomal Ca^{2+} content in drug-treated samples relative to controls assessed after GPN addition, or decreases in LysoTracker® signals on initial drug addition ('lysosomotropism' [28,29]) were regarded as more generalized actions of the drug candidates on the lysosomal Ca^{2+} stores distinct from activity against the NAADP-evoked Ca^{2+} release pathway. Representative traces showing ratios (F/F₀) of green (fluo-4) and red (LysoTracker®) fluorescence signals over time are shown in Fig. 5A for several of the candidates (examples lacking and displaying effects) and controls (vehicle, no GPN, bafilomycin and a protease inhibitor cocktail to impair GPN action). Several of the candidate drugs (for example, prochlorperazine and trifluoperazine in Fig. 5A) caused a rapid decrease in LysoTracker® staining (Fig. 5A, bottom) and a decrease in mobilizable lysosomal Ca^{2+} content on GPN addition (Fig. 5A, top). These effects were related, with a strong observed correlation between loss of LysoTracker® staining and GPN-evoked Ca^{2+} transient amplitude (Fig. 5B). Data from the portfolio of all 18 candidates are shown in Fig. 5B, identifying three broad groupings – (i) compounds with no effect on LysoTracker® or GPN signal intensity, clustering with negative controls (water, DMSO; boxed in Fig. 5B), (ii) compounds with penetrant effects on both LysoTracker® and GPN signal intensity (the positive control bafilomycin, and several phenothiazines: prochlorperazine (rank #9),

thioridazine (rank #10) and trifluoperazine (rank #18) and (iii) a group of 8 compounds with a profile intermediate between these groupings (~30-50% decrease in fluorescence ratio versus controls). Only the seven candidates with no effect on GPN-mobilizable Ca^{2+} or LTR staining - the first grouping, PF-543 (rank #1), SKF96365 (rank #2), racecadotril (rank #5), A-315456 (rank #6), LY-310,762 (rank #12), PDMP (rank #15) and salmeterol (rank #16) - were advanced for further validation. The remaining 11 candidates were not pursued further in the context of this study (shaded rows in Table 1).

3.3. Validation of candidates against NAADP-dependent processes in mammalian cells

The effects of the remaining seven candidates on the amplitude of NAADP-evoked Ca^{2+} signals in human U2OS cells was examined. These experiments were performed by monitoring Ca^{2+} release kinetics following microinjection of NAADP into single cells (Fig. 6). Whereas injection of buffer alone evoked only a small stimulus artefact, injection of NAADP evoked a robust Ca^{2+} transient (peak F/F₀ = 4.0 ± 0.6, n = 3 injections, Fig. 6A). The action of NAADP was then examined in cells preincubated with the candidate inhibitors (10μM, 10 min pretreatment), as well as other compounds of interest. PPADS – the positive control NAADP inhibitor from sea urchin assays [31] - decreased the amplitude of the NAADP-evoked Ca^{2+} transient to 24.2 ± 2.1% of control values (Fig. 6A). However, neither ned-19, nor naringenin significantly attenuated Ca^{2+} signal amplitude following NAADP microinjection (Fig. 6A). Examination of each candidate inhibitor revealed varying degrees of inhibition of NAADP-evoked Ca^{2+} responses under the preincubation conditions (10μM) with the most effective compounds being SKF96365 (12.4 ± 8.9% of control values), PF-543 (14.1 ± 3.0% of control values) and racecadotril (16.6 ± 10% of control values). These compounds were highly ranked in the sea urchin screen (SKF96365 (rank #2), PF-543 (rank #1) and racecadotril (rank #5)) and compared well with PPADS (24.2 ± 2.1% of control values). PDMP (rank #15) caused the lowest extent of inhibition
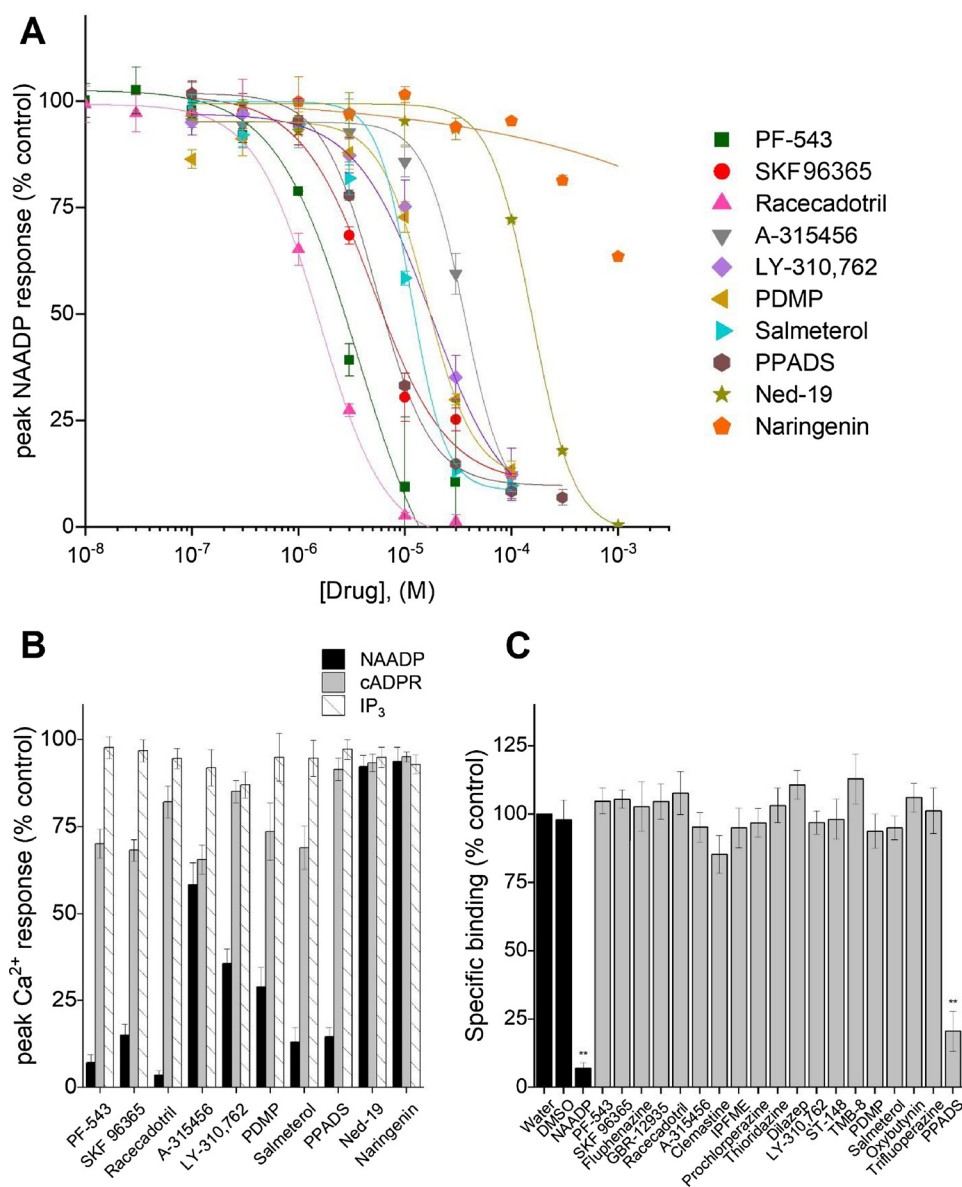
Fig. 4. Secondary validation of candidates in sea urchin egg homogenate. A, Full concentration response curves resolving effects of selected primary screen candidates on Ca^{2+} release in sea urchin egg homogenates evoked by NAADP (70 nM). Current NAADP antagonists (PPADS, ned-19 and naringenin) are also included. IC_{50} values for the entire dataset are provided in Table 1. B, Averaged peak Ca^{2+} release in the presence of drug (30 μM, 5 min preincubation time) relative to vehicle controls, in response to EC_{70} concentrations of NAADP (70 nM), cADPR (100 nM), or IP_3 (200 nM). C, Analysis of effects of all 18 candidates on specific ^{32}P-NAADP radioligand binding levels in the presence of drug (30 μM), relative to vehicle controls. p-values: ** p < 0.01 relative to DMSO controls.

(43.7 ± 15.0% of control values) which was none-the-less still a considerable improvement over both ned-19 and naringenin in our hands.

Finally, in the companion paper [25], we had established that inhibition of either NAADP-sensitive Ca^{2+} release, or TPC1/TPC2 activity, impaired the translocation of a MERS pseudovirus through the endolysosomal system. The unbiased screening approach described here generated an additional panel of inhibitors of NAADP-evoked Ca^{2+} signaling. Therefore, the potential effectiveness of these compounds in the MERS pseudovirus infectivity assay was assessed. Results from this MERS pseudovirus bioassay were plotted along with the Ca^{2+} release inhibition data in Fig. 6B. Visual inspection of the results from both datasets revealed a strong correlation between results from these independent assays, further supporting the conclusions of the companion paper that ligands targeting the NAADP pathway inhibit MERS pseudovirus translocation [25], while highlighting new scaffolds for manipulation of NAADP-dependent signaling processes in mammalian cells.

4. Discussion

Here we have performed a 'proof of principle' unbiased screen in the sea urchin egg homogenate system with the goal of using this system as

an entry point to a validation pipeline aimed at discovering novel chemical scaffolds to inhibit NAADP-evoked Ca^{2+} release. Discovery of modulators of NAADP-evoked Ca^{2+} signaling is important as appreciation grows of the role of this pathway in (dys)regulating cellular processes [11,14–23]. There is certainly room for improvement in defining ligands with improved selectivity and reliable activity against the NAADP signaling pathway.

The small pilot screen (1534 compounds) was robust in terms of signal amplitude (Fig. 2), the population spread of inhibitory values (Fig. 3B) and most importantly success in identifying known blockers of NAADP-evoked Ca^{2+} release within the screened inventory. Examples of such compounds which ranked highly in the primary screen include (i) [^{32}P]-NAADP binding inhibitors, PPNDS (primary screen rank #27, [31]) and PPADS (rank #62 [31]), and (ii) previously identified Ca_v blockers, nicardipine (rank #35, [32]), diltiazem (rank #113 [32]), verapamil (rank #120 [32]), and nifedipine (rank #149 [32]). Other Ca_v modulators found within the top hundred 'hits' included FPL64176 (rank #34), nitrendipine (rank #85) and methoxyverapamil (rank #95), as well as the highly ranked hit SKF96365 (rank #2, discussed below [50,51]). These Ca_v blockers would be predicted to serve as TPC pore blockers, as supported by virtual docking analyses and microinjection studies [13].
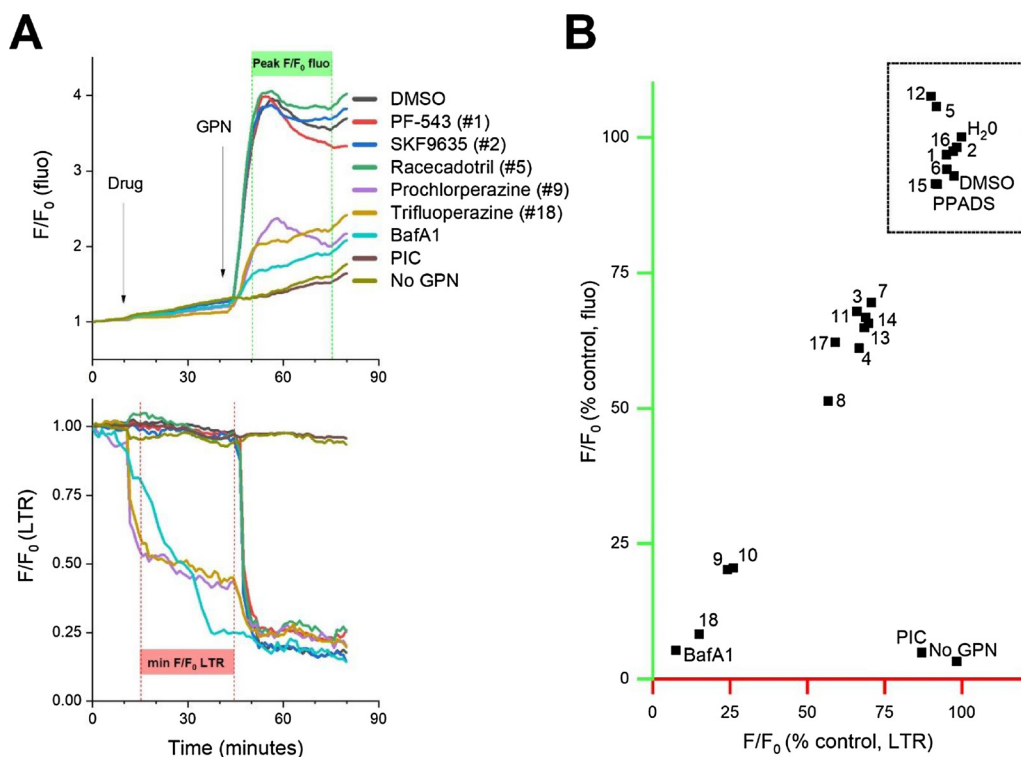
Fig. 5. Characterization of candidate inhibitors on lysosomal Ca^{2+} stores in U2OS cells. **A**, representative traces of GPN induced Ca^{2+} release (top) and lysosomal disruption (bottom). U2OS cells were loaded with Fluo-4 AM and LysoTracker® Red (LTR). Baseline fluorescence values were recorded for 15 min before addition of test compounds (30μM). Fluorescence was then monitored for 40 min before addition of GPN (300μM) to release lysosomal Ca^{2+}. Measurements were made to quantify GPN evoked Ca^{2+} release (top) and loss of LTR fluorescence following initial drug addition (bottom) by assessing fluorescence ratio values in the regions highlighted by the green (peak F/F_o ratio) and red bars (minimal F/F_o ratio). PIC, protease inhibitor cocktail; BafA1, bafilomycin A1. **B**, Correlation plot depicting relationship between measurements of GPN induced calcium release (*y*-axis, green) and drug-induced lysosome disruption (*x*-axis red). Values are replotted from highlighted regions in (A). The cluster of non-lysomotropic compounds is highlighted (box). Data represents peak fluo-4 fluorescence ratios (F_{fluo}/F_0, where 'F_{fluo}' represents fluo-4 fluorescence at peak, and F_0 represents fluorescence at time = 0) and minimum LysoTracker® fluorescence ratios (F_{LTR}/F_0, where 'F_{LTR}' represents minimum LysoTracker® Red fluorescence prior to GPN addition, and F_0 represents fluorescence at time = 0). Compounds are labeled according to ranking # in Table 1.

Here, we prioritized candidates showing ≥80% inhibition of the peak NAADP-evoked Ca^{2+} signal. This comprised eighteen candidates, seven of which progressed through validation in subsequent assays. This 'hit' proportion (~0.5% from 1534 compounds) is consistent with discovery rates observed in other screens, and is especially agreeable given the low execution cost for the urchin screening platform. Prior reticence to use this system for unbiased screening may have related to concern over tractability of structure-activity relationships from the urchin to human pathways. Differences in sensitivities between sea urchin and mammalian systems have previously been noted for structural analogs of NAADP [42] implying differences in NAADP binding protein specificity [45,52]. However, this relates to finer structure-activity relationships within defined chemical series, rather than discovery of new scaffolds. While obviously data reflects the sensitivities and specificities of an invertebrate Ca^{2+} release system, the utility of C. elegans and Drosophila as drug screening models is noted [57]. In our opinion, the advantages of high assay throughput in the sea urchin system offsets the need for subsequent validation of 'hits' against NAADP-evoked responses in human cells. Even so a similar ordering of potency was ultimately observed between the sea urchin and human cell bioassays: SKF96365, PF-543 and racecadotril were the most penetrant inhibitors in both systems (Fig. 4, Table 1). Identification of these three novel hits (Table 1) that (i) inhibited Ca^{2+} release by > 80% in a human cell line, more than seen with tetrandrine under identical conditions [25], (ii) reduced MERS pseudovirus translocation to levels observed with fangchinoline (Fig. 1, [58]), and (iii) lacked demonstrable action in the counterscreen provides strong support for execution of a higher throughput screening campaign using sea urchin egg homogenate. Screening large compound libraries against endogenous NAADP-evoked signals mediated via TPCs *within their acidic store native environment* in mammalian cells would be a much more daunting prospect. Screens of TPCs targeted to the cell surface [59], or virtual screens based upon TPC recent structures [60–62] represent viable, complementary approaches.

Deprioritization of the other original candidates (11/18 'hits') during the validation pipeline was attributable to generalized effects on the acidic Ca^{2+} stores, experimentally monitored as decreased LTR fluorescence intensity or GPN-evoked Ca^{2+} release (> 30% decrease as cutoff, Table 1 & Fig. 5). Numerous compounds and chemical scaffolds have been shown to accumulate within the acidic Ca^{2+} store lumen where they can modulate (e.g. functional inhibitors of acid sphingomyelinase, FIASMAs [63,64]) or act as substrates of luminal enzymes [65] to alter the structure and/or function and even integrity of the lysosome (e.g. osmotic lysis by GPN). Examples of compounds dropped from the pipeline based on counter-screening assays, that are known to fall within this category [63,66] are multiple phenothiazine compounds (rank #3, #9, #10, #18), clemastine (rank #7) and dilazep (rank #11). These compounds display higher lipophilicity (average *ClogP*, 4.85) and basic pKa (average pKa, 8.9) than the remaining dataset. Other excluded compounds (GBR-12935, IPFME, ST-148, TMB-8 and oxybutynin) are new lysosomotropic suspects. This does not equate to a lack of usefulness as research tools, or even clinical drugs, as many approved therapeutics show marked lysosomotropism, a feature that may actually contribute to their clinical efficacy [63,67,68]. This is especially relevant for novel uses of existing clinical agents to target pathogens that traverse the endolysosomal system, where drug accumulation with acidic Ca^{2+} stores would be a desirable attribute for pathogen targeting [25,69]. Such activities may have good repurposing potential, but for our purposes here, inhibition of NAADP-evoked Ca^{2+} release by these candidates is likely indirect.

The seven candidates advanced through the pilot screen pipeline deserve further scrutiny. All inhibited NAADP evoked Ca^{2+} signals responses in the human cell line (Fig. 6) under conditions less penetrant than the counterscreen where no changes in lysosomal properties were observed (Fig. 5). The three top ranked hits - SKF96365, PF-543 and racecadotril – have not previously been shown to impair NAADP-evoked Ca^{2+} signaling. None of these compounds interfered with specific ^{32}P-NAADP binding implying inhibition through other
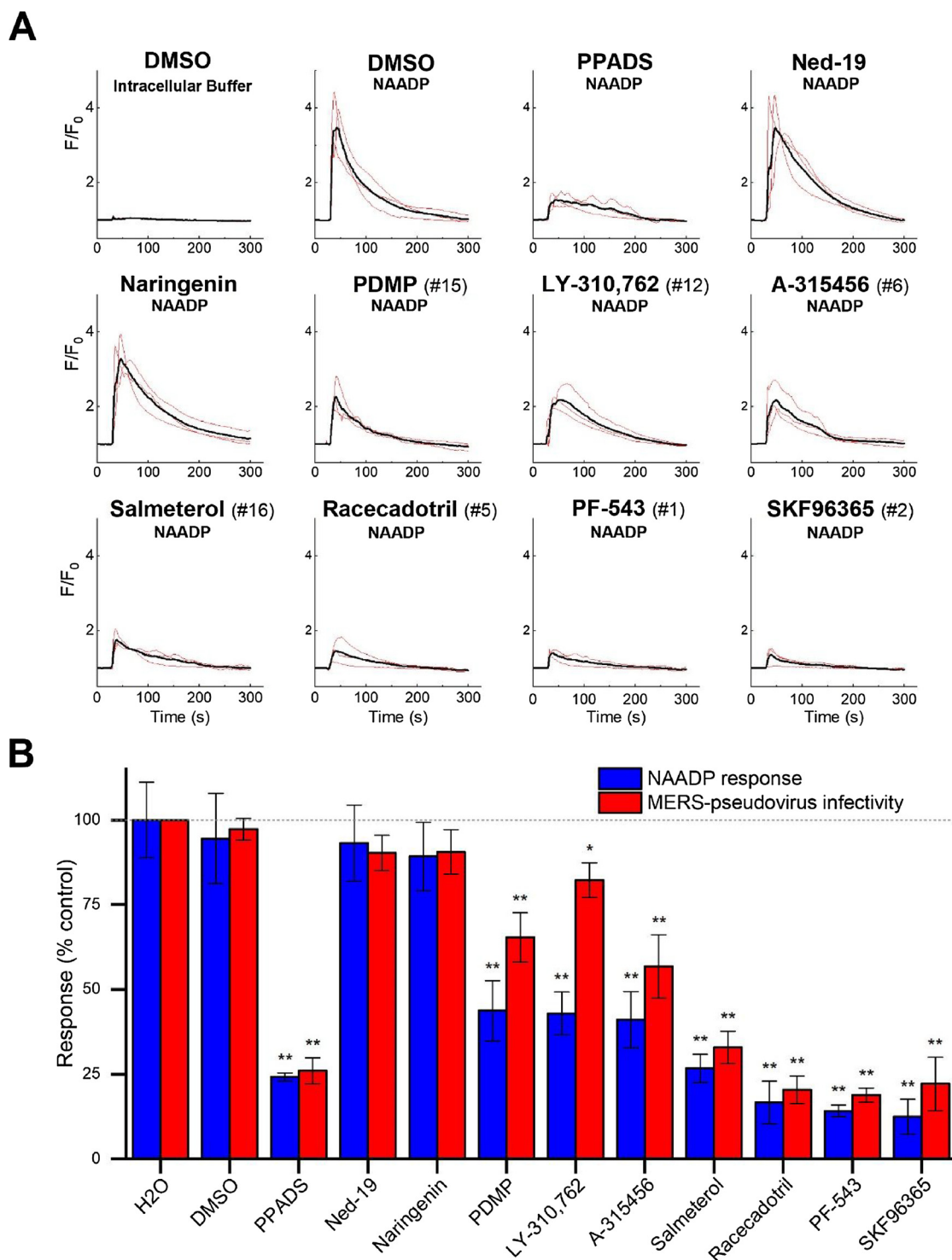
Fig. 6. Validation of NAADP-inhibitors in mammalian cells. **A,** Ca^{2+} traces resolved by fluo-4 fluorescence in response to NAADP microinjection (100 nM pipette concentration) in U2OS cells treated with indicated drugs (10μM, 10 min pretreatment). Individual traces shown in red, averaged response shown in black. **B,** Quantification of peak amplitude of NAADP-evoked Ca^{2+} transients in microinjected U2OS cells relative to control (blue bars) following preincubation with indicated drugs as shown in (A). Red bars report luciferase levels in a MERS-pseudovirus cell translocation assay in Huh7 cells relative to controls (H_2O, DMSO) following treatment with the same panel of drugs (10μM for 1 h prior to exposure to MERS-pseudovirus for a 5 h period). MERS-pseudovirus cell entry was detected 3 days post infection by measuring luciferase activity as described fully in the companion paper [25]. p-values: * $p < 0.05$, ** $p < 0.01$ relative to DMSO controls.

mechanisms (Fig. 4C). SKF96365 is a low voltage-activated T-type Ca_v blocker, with antagonist action at other Ca_vs and TRPC channels [50,51]. This polypharmacological profile may now extend to TPCs. Direct electrophysiological analysis will be needed to confirm if the observed inhibition of NAADP action in Ca^{2+}-free extracellular media by SKF96365 (Fig. 6A) results from TPC pore blocking ability. Our data

also suggest caution in attribution of the mechanistic basis of effects of SKF96365 in studies of Ca^{2+} signaling [70]. PF-543 is a cell-permeant inhibitor of sphingosine kinase [49], application of which causes a dose-dependent increases in cellular sphingosine levels. Elevated sphingosine levels attenuate acidic Ca^{2+} store signaling, as evidenced by impaired responses to NAADP in patients with Niemann-Pick type

C1 disease [71]. This inhibition may be caused by sphingosine-dependent TPC1 activation [72], impaired lysosomal Ca^{2+} uptake and/or lysosomal permeabilization [65,71]. Action of PF-543 through any of these mechanisms would result in the observed inhibition of NAADP-evoked Ca^{2+} signals. Racecadotril (acetorphan) is a neutral endopeptidase inhibitor (NEP), used therapeutically as an antidiarrheal agent by blocking enkephalin-mediated intestinal fluid secretion. It is also a prodrug, being rapidly converted to thiorphan, a low nanomolar NEP inhibitor. Inhibition of neprilysin (an amyloid β (Aβ) peptide degrading enzyme) by infusion of thiorphan in a mouse model of Alzheimer's disease is associated with extensive lysosomal accumulation of Aβ as well as changes in lysosomal number and size [73]. These data evidence lysosomal alterations which, as seen in other neurodegenerative models [18], dysregulate NAADP action. Further experiments will be needed to define mechanistically how these drugs impair NAADP action.

In conclusion, interrogation of the sea urchin egg homogenate platform provided new leads for inhibiting NAADP-dependent processes - NAADP-evoked Ca^{2+} signaling, as well as MERS pseudovirus infectivity – in human cells. Even though only a small number of compounds were profiled in this initial unbiased pilot screen, the effectiveness of the highly ranked compounds was as good as achieved through structure-activity based screening around the known tetrandrine scaffold (see companion study, [25]). These data provide strong support for execution of a higher throughput screening campaign using the sea urchin egg homogenate system to discover new ligands for manipulation of NAADP signaling, as well as for modulators of cADPR and IP_3 action.

Conflicts of interest

None.

Appendix A. Supplementary data

Supplementary material related to this article can be found, in the online version, at doi:https://doi.org/10.1016/j.ceca.2018.08.002.

References

[1] A.J. Morgan, F.M. Platt, E. Lloyd-Evans, A. Galione, Molecular mechanisms of endolysosomal Ca^{2+} signalling in health and disease, Biochem. J. 439 (2011) 349–374.

[2] H.C. Lee, Nicotinic acid adenine dinucleotide phosphate (NAADP)-mediated calcium signaling, J. Biol. Chem. 280 (2005) 33693–33696.

[3] A. Galione, A primer of NAADP-mediated $Ca(2+)$ signalling: from sea urchin eggs to mammalian cells, Cell Calcium 58 (2015) 27–47.

[4] E. Brailoiu, D. Churamani, X. Cai, M.G. Schrlau, G.C. Brailoiu, X. Gao, R. Hooper, M.J. Boulware, N.J. Dun, J.S. Marchant, S. Patel, Essential requirement for two-pore channel 1 in NAADP-mediated calcium signaling, J. Cell Biol. 186 (2009) 201–209.

[5] P.J. Calcraft, M. Ruas, Z. Pan, X. Cheng, A. Arredouani, X. Hao, J. Tang, K. Rietdorf, L. Teboul, K.T. Chuang, P. Lin, R. Xiao, C. Wang, Y. Zhu, Y. Lin, C.N. Wyatt, J. Parrington, J. Ma, A.M. Evans, A. Galione, M.X. Zhu, NAADP mobilizes calcium from acidic organelles through two-pore channels, Nature 459 (2009) 596–600.

[6] X. Zong, M. Schieder, H. Cuny, S. Fenske, C. Gruner, K. Rotzer, O. Griesbeck, H. Harz, M. Biel, C. Wahl-Schott, The two-pore channel TPCN2 mediates NAADP-dependent $Ca(2+)$-release from lysosomal stores, Pflugers Arch. 458 (2009) 891–899.

[7] A. Jha, M. Ahuja, S. Patel, E. Brailoiu, S. Muallem, Convergent regulation of the lysosomal two-pore channel-2 by $Mg(2)(+)$, NAADP, $PI(3,5)P(2)$ and multiple protein kinases, EMBO J. 33 (2014) 501–511.

[8] M. Ruas, L.C. Davis, C.C. Chen, A.J. Morgan, K.T. Chuang, T.F. Walseth, C. Grimm,

[9] C. Garnham, T. Powell, N. Platt, F.M. Platt, M. Biel, C. Wahl-Schott, J. Parrington, A. Galione, Expression of $Ca(2+)$-permeable two-pore channels rescues NAADP signalling in TPC-deficient cells, EMBO J. 34 (2015) 1743–1758.

[9] A.J. Morgan, L.C. Davis, M. Ruas, A. Galione, TPC: the NAADP discovery channel? Biochem. Soc. Trans. 43 (2015) 384–389.

[10] X. Wang, X. Zhang, X.P. Dong, M. Samie, X. Li, X. Cheng, A. Goschka, D. Shen, Y. Zhou, J. Harlow, M.X. Zhu, D.E. Clapham, D. Ren, H. Xu, TPC proteins are phosphoinositide- activated sodium-selective ion channels in endosomes and lysosomes, Cell 151 (2012) 372–383.

[11] C. Cang, Y. Zhou, B. Navarro, Y.J. Seo, K. Aranda, L. Shi, S. Battaglia-Hsu, I. Nissim, D.E. Clapham, D. Ren, mTOR regulates lysosomal ATP-sensitive two-pore $Na(+)$ channels to adapt to metabolic state, Cell 152 (2013) 778–790.

[12] E. Brailoiu, R. Hooper, X. Cai, G.C. Brailoiu, M.V. Keebler, N.J. Dun, J.S. Marchant, S. Patel, An ancestral deuterostome family of two-pore channels mediates nicotinic acid adenine dinucleotide phosphate-dependent calcium release from acidic organelles, J. Biol. Chem. 285 (2009) 2897–2901.

[13] T. Rahman, X. Cai, G.C. Brailoiu, M.E. Abood, E. Brailoiu, S. Patel, Two-pore channels provide insight into the evolution of voltage-gated Ca^{2+} and Na^+ channels, Sci. Signal. 7 (2014) ra109.

[14] C. Grimm, C.C. Chen, C. Wahl-Schott, M. Biel, Two-pore channels: catalyzers of endolysosomal transport and function, Front. Pharmacol. 8 (2017) 45.

[15] C. Grimm, E. Butz, C.C. Chen, C. Wahl-Schott, M. Biel, From mucolipidosis type IV to Ebola: TRPML and two-pore channels at the crossroads of endo-lysosomal trafficking and disease, Cell Calcium 67 (2017) 148–155.

[16] S. Patel, Function and dysfunction of two-pore channels, Sci. Signal. 8 (2015) re7.

[17] Y. Sakurai, A.A. Kolokoltsov, C.C. Chen, M.W. Tidwell, W.E. Bauta, N. Klugbauer, C. Grimm, C. Wahl-Schott, M. Biel, R.A. Davey, Ebola virus. Two-pore channels control Ebola virus host cell entry and are drug targets for disease treatment, Science 347 (2015) 995–998.

[18] L. Hockey, B.S. Kilpatrick, E.R. Eden, Y. Lin-Moshier, G.C. Brailoiu, E. Brailoiu, C.E. Futter, A.H. Schapira, J.S. Marchant, S. Patel, Dysregulation of lysosomal morphology by pathogenic LRRK2 is corrected by two-pore channel inhibition, J Cell Science 128 (2015) 232–238.

[19] J.J. Kelu, S.E. Webb, J. Parrington, A. Galione, A.L. Miller, $Ca(2+)$ release via two-pore channel type 2 (TPC2) is required for slow muscle cell myofibrillogenesis and myotomal patterning in intact zebrafish embryos, Dev. Biol. 425 (2017) 109–129.

[20] R.A. Capel, E.L. Bolton, W.K. Lin, D. Aston, Y. Wang, W. Liu, X. Wang, R.A. Burton, D. Bloor-Young, K.T. Shade, M. Ruas, J. Parrington, G.C. Churchill, M. Lei, A. Galione, D.A. Terrar, Two-pore channels (TPC2s) and nicotinic acid adenine dinucleotide phosphate (NAADP) at lysosomal-sarcoplasmic reticular junctions contribute to acute and chronic beta-adrenoceptor signaling in the heart, J. Biol. Chem. 290 (2015) 30087–30098.

[21] P.H. Lin, P. Duann, S. Komazaki, K.H. Park, H. Li, M. Sun, M. Sermersheim, K. Gumpper, J. Parrington, A. Galione, A.M. Evans, M.X. Zhu, J. Ma, Lysosomal two-pore channel subtype 2 (TPC2) regulates skeletal muscle autophagic signaling, J. Biol. Chem. (2014).

[22] P.V. Lear, D. Gonzalez-Touceda, B. Porteiro Couto, P. Viano, V. Guymer, E. Remzova, R. Tunn, A. Chalasani, T. Garcia-Caballero, I.P. Hargreaves, P.W. Tynan, H.C. Christian, R. Nogueiras, J. Parrington, C. Dieguez, Absence of intracellular ion channels TPC1 and TPC2 leads to mature-onset obesity in male mice, due to impaired lipid availability for thermogenesis in brown adipose tissue, Endocrinology 156 (2015) 975–986.

[23] C. Grimm, L.M. Holdt, C.C. Chen, S. Hassan, C. Muller, S. Jors, H. Cuny, S. Kissing, B. Schroder, E. Butz, B. Northoff, J. Castonguay, C.A. Luber, M. Moser, S. Spahn, R. Lullmann-Rauch, C. Fendel, N. Klugbauer, O. Griesbeck, A. Haas, M. Mann, F. Bracher, D. Teupser, P. Saftig, M. Biel, C. Wahl-Schott, High susceptibility to fatty liver disease in two-pore channel 2-deficient mice, Nat. Commun. 5 (2014) 4699.

[24] P. Suarez-Cortes, G. Gambara, A. Favia, F. Palombi, P. Alano, A. Filippini, Ned-19 inhibition of parasite growth and multiplication suggests a role for NAADP mediated signalling in the asexual development of Plasmodium falciparum, Malar. J. 16 (2017) 366.

[25] G. Gunaratne, Y. Yang, F. Li, T.F. Walseth, J.S. Marchant, Inhibition of Two-Pore channels blocks Middle East Respiratory Syndrome Coronavirus translocation through the endolysosomal system, Companion Pap. (2018).

[26] A. Favia, M. Desideri, G. Gambara, A. D'Alessio, M. Ruas, B. Esposito, D. Del Bufalo, J. Parrington, E. Ziparo, F. Palombi, A. Galione, A. Filippini, VEGF-induced neoangiogenesis is mediated by NAADP and two-pore channel-2-dependent $Ca2+$ signaling, Proc. Natl. Acad. Sci. U. S. A. 111 (2014) E4706–E4715.

[27] I. Pafumi, M. Festa, F. Papacci, L. Lagostena, C. Giunta, V. Gutla, L. Cornara, A. Favia, F. Palombi, F. Gambale, A. Filippini, A. Carpaneto, Naringenin impairs two-pore channel 2 activity and inhibits VEGF-induced angiogenesis, Sci. Rep. 7 (2017) 5121.

[28] C. de Duve, T. de Barsy, B. Poole, A. Trouet, P. Tulkens, F. Van Hoof, Commentary. Lysosomotropic agents, Biochem. Pharmacol. 23 (1974) 2495–2531.

[29] B. Lemieux, M.D. Percival, J.P. Falgueyret, Quantitation of the lysosomotropic character of cationic amphiphilic drugs using the fluorescent basic amine Red DND-99, Anal. Biochem. 327 (2004) 247–251.

[30] E. Naylor, A. Arredouani, S.R. Vasudevan, A.M. Lewis, R. Parkesh, A. Mizote, D. Rosen, J.M. Thomas, M. Izumi, A. Ganesan, A. Galione, G.C. Churchill, Identification of a chemical probe for NAADP by virtual screening, Nat. Chem. Biol. 5 (2009) 220–226.

[31] R.A. Billington, A.A. Genazzani, PPADS is a reversible competitive antagonist of the NAADP receptor, Cell Calcium 41 (2007) 505–511.

[32] A.A. Genazzani, M. Mezna, D.M. Dickey, F. Michelangeli, T.F. Walseth, A. Galione, Pharmacological properties of the $Ca2+$-release mechanism sensitive to NAADP in the sea urchin egg, Br. J. Pharmacol. 121 (1997) 1489–1495.

[33] J. Dowden, G. Berridge, C. Moreau, M. Yamasaki, G.C. Churchill, B.V. Potter, A. Galione, Cell-permeant small-molecule modulators of NAADP-mediated Ca2+ release, Chem. Biol. 13 (2006) 659–665.

[34] H.C. Lee, R. Aarhus, T.F. Walseth, Calcium mobilization by dual receptors during fertilization of sea-urchin eggs, Science 261 (1993) 352–355.

[35] H.C. Lee, R. Aarhus, A derivative of NADP mobilizes calcium stores insensitive to inositol trisphosphate and cyclic ADP-ribose, J. Biol. Chem. 270 (1995) 2152–2157.

[36] A. Galione, K.T. Chuang, T.M. Funnell, L.C. Davis, A.J. Morgan, M. Ruas, J. Parrington, G.C. Churchill, Preparation and use of sea urchin egg homogenates for studying NAADP-mediated Ca(2)(+) release, Cold Spring Harb. Protoc. 2014 (2014) 988–992.

[37] A.J. Morgan, K. Bampali, M. Ruas, C. Factor, T.G. Back, S.R.W. Chen, A. Galione, Carvedilol inhibits cADPR- and IP3-induced Ca(2+) release, Messenger (Los Angel) 5 (2016) 92–99.

[38] S.R. Vasudevan, N. Singh, G.C. Churchill, Scaffold hopping with virtual screening from IP3 to a drug-like partial agonist of the inositol trisphosphate receptor, Chembiochem 15 (2014) 2774–2782.

[39] R.A. Billington, J. Bak, A. Martinez-Coscolla, M. Debidda, A.A. Genazzani, Triazine dyes are agonists of the NAADP receptor, Br. J. Pharmacol. 142 (2004) 1241–1246.

[40] P. Jain, J.T. Slama, L.A. Perez-Haddock, T.F. Walseth, Nicotinic Acid Dinucleotide Phosphate Analogs containing substituted nicotinic acid: effect of modification on Ca^{2+} release, J. Med. Chem. 53 (2010) 7599–7612.

[41] D. Rosen, A.M. Lewis, A. Mizote, J.M. Thomas, P.K. Aley, S.R. Vasudevan, R. Parkesh, A. Galione, M. Izumi, A. Ganesan, G.C. Churchill, Analogues of the nicotinic acid adenine dinucleotide phosphate (NAADP) indicate two binding sites on the NAADP receptor, J. Biol. Chem. 284 (2009) 34930–34934.

[42] R.A. Ali, T. Zhelay, C.J. Trabbic, T.F. Walseth, J.T. Slama, D.R. Giovannucci, K.A. Wall, Activity of nicotinic acid substituted nicotinic acid adenine dinucleotide phosphate (NAADP) analogs in a human cell line: difference in specificity between human and sea urchin NAADP receptors, Cell Calcium 55 (2014) 93–103.

[43] T.F. Walseth, H.C. Lee, Synthesis and characterization of antagonists of cyclic-ADP-ribose-induced Ca^{2+} release, Biochim. Biophys. Acta 1178 (1993) 235–242.

[44] D.L. Clapper, T.F. Walseth, P.J. Dargie, H.C. Lee, Pyridine nucleotide metabolites stimulate calcium release from sea urchin egg microsomes desensitized to inositol trisphosphate, J. Biol. Chem. 262 (1987) 9561–9568.

[45] T.F. Walseth, Y. Lin-Moshier, P. Jain, M. Ruas, J. Parrington, A. Galione, J.S. Marchant, J.T. Slama, Photoaffinity labeling of high affinity nicotinic acid adenine dinucleotide phosphate (NAADP)-binding proteins in sea urchin egg, J. Biol. Chem. 287 (2012) 2308–2315.

[46] R. Aarhus, D.M. Dickey, R.M. Graeff, K.R. Gee, T.F. Walseth, H.C. Lee, Activation and inactivation of Ca2+ release by NAADP+, J. Biol. Chem. 271 (1996) 8513–8516.

[47] J.H. Zhang, T.D. Chung, K.R. Oldenburg, A simple statistical parameter for use in evaluation and validation of high throughput screening assays, J. Biomol. Screen. 4 (1999) 67–73.

[48] D.M. Dickey, R. Aarhus, T.F. Walseth, H.C. Lee, Thio-NADP is not an antagonist of NAADP, Cell Biochem. Biophys. 28 (1998) 63–73.

[49] M.E. Schnute, M.D. McReynolds, T. Kasten, M. Yates, G. Jerome, J.W. Rains, T. Hall, J. Chrencik, M. Kraus, C.N. Cronin, M. Saabye, M.K. Highkin, R. Broadus, S. Ogawa, K. Cukyne, L.E. Zawadzke, V. Peterkin, K. Iyanar, J.A. Scholten, J. Wendling, H. Fujiwara, O. Nemirovskiy, A.J. Wittwer, M.M. Nagiec, Modulation of cellular S1P levels with a novel, potent and specific inhibitor of sphingosine kinase-1, Biochem. J. 444 (2012) 79–88.

[50] A. Singh, M.E. Hildebrand, E. Garcia, T.P. Snutch, The transient receptor potential channel antagonist SKF96365 is a potent blocker of low-voltage-activated T-type calcium channels, Br. J. Pharmacol. 160 (2010) 1464–1475.

[51] J.E. Merritt, W.P. Armstrong, C.D. Benham, T.J. Hallam, R. Jacob, A. Jaxa-Chamiec, B.K. Leigh, S.A. McCarthy, K.E. Moores, T.J. Rink, SK&F 96365, a novel inhibitor of receptor-mediated calcium entry, Biochem. J. 271 (1990) 515–522.

[52] Y. Lin-Moshier, T.F. Walseth, D. Churamani, S.M. Davidson, J.T. Slama, R. Hooper, E. Brailoiu, S. Patel, J.S. Marchant, Photoaffinity labeling of nicotinic acid adenine dinucleotide phosphate (NAADP) targets in mammalian cells, J. Biol. Chem. 287 (2012) 2296–2307.

[53] T.F. Walseth, Y. Lin-Moshier, K. Weber, J.S. Marchant, J.T. Slama, A.H. Guse, Nicotinic acid adenine dinucleotide 2'-phosphate binding proteins in t lymphocytes, Messenger 1 (2012) 86–94.

[54] J.S. Marchant, Y. Lin-Moshier, T. Walseth, S. Patel, The molecular basis for Ca^{2+}

[55] signalling by NAADP: two-pore channels in a complex? Messenger 1 (2012) 63–76.

[55] T.O. Berg, E. Stromhaug, T. Lovdal, O. Seglen, T. Berg, Use of glycyl-L-phenylalanine 2-naphthylamide, a lysosome-disrupting cathepsin C substrate, to distinguish between lysosomes and prelysosomal endocytic vacuoles, Biochem. J. 300 (Pt 1) (1994) 229–236.

[56] Z. Padamsey, L. McGuinness, S.J. Bardo, M. Reinhart, R. Tong, A. Hedegaard, M.L. Hart, N.J. Emptage, Activity-dependent exocytosis of lysosomes regulates the structural plasticity of dendritic spines, Neuron 93 (2017) 132–146.

[57] K. Strange, Drug discovery in fish, flies, and worms, ILAR J. 57 (2016) 133–143.

[58] G. Gunaratne, M.E. Johns, T.F. Walseth, J.S. Marchant, A screening campaign in sea urchin egg homogenate as a platform for discovering modulators of NAADP-dependent Ca^{2+} signals in human cells, Companion Pap. (2018).

[59] E. Brailoiu, T. Rahman, D. Churamani, D.L. Prole, G.C. Brailoiu, R. Hooper, C.W. Taylor, S. Patel, An NAADP-gated two-pore channel targeted to the plasma membrane uncouples triggering from amplifying Ca^{2+} signals, J. Biol. Chem. 285 (2010) 38511–38516.

[60] J. Guo, W. Zeng, Q. Chen, C. Lee, L. Chen, Y. Yang, C. Cang, D. Ren, Y. Jiang, Structure of the voltage-gated two-pore channel TPC1 from Arabidopsis thaliana, Nature 531 (2016) 196–201.

[61] A.F. Kintzer, R.M. Stroud, Structure, inhibition and regulation of two-pore channel TPC1 from Arabidopsis thaliana, Nature 531 (2016) 258–262.

[62] J. She, J. Guo, Q. Chen, W. Zeng, Y. Jiang, X.C. Bai, Structural insights into the voltage and phospholipid activation of the mammalian TPC1 channel, Nature 556 (2018) 130–134.

[63] J. Kornhuber, M. Muehlbacher, S. Trapp, S. Pechmann, A. Friedl, M. Reichel, C. Muhle, L. Terfloth, T.W. Groemer, G.M. Spitzer, K.R. Liedl, E. Gulbins, P. Tripal, Identification of novel functional inhibitors of acid sphingomyelinase, PLoS One 6 (2011) e23852.

[64] J. Kornhuber, P. Tripal, M. Reichel, C. Muhle, C. Rhein, M. Muehlbacher, T.W. Groemer, E. Gulbins, Functional Inhibitors of Acid Sphingomyelinase (FIASMAs): a novel pharmacological group of drugs with broad clinical applications, Cell. Physiol. Biochem. 26 (2010) 9–20.

[65] A.M. Villamil Giraldo, H. Appelqvist, T. Ederth, K. Ollinger, Lysosomotropic agents: impact on lysosomal membrane permeabilization and cell death, Biochem. Soc. Trans. 42 (2014) 1460–1464.

[66] S. Nadanaciva, S. Lu, D.F. Gebhard, B.A. Jessen, W.D. Pennie, Y. Will, A high content screening assay for identifying lysosomotropic compounds, Toxicol. In Vitro 25 (2011) 715–723.

[67] E. Gulbins, M. Palmada, M. Reichel, A. Luth, C. Bohmer, D. Amato, C.P. Muller, C.H. Tischbirek, T.W. Groemer, G. Tabatabai, K.A. Becker, P. Tripal, S. Staedtler, T.F. Ackermann, J. van Brederode, C. Alzheimer, M. Weller, U.E. Lang, B. Kleuser, H. Grassme, J. Kornhuber, Acid sphingomyelinase-ceramide system mediates effects of antidepressant drugs, Nat. Med. 19 (2013) 934–938.

[68] H.Y. Chung, C.J. Witt, N. Jbeily, J. Hurtado-Oliveros, B. Giszas, A. Lupp, M.H. Graler, T. Bruns, A. Stallmach, F.A. Gonnert, R.A. Claus, Acid sphingomyelinase inhibition prevents development of Sepsis sequelae in the murine liver, Sci. Rep. 7 (2017) 12348.

[69] J. Dyall, C.M. Coleman, B.J. Hart, T. Venkataraman, M.R. Holbrook, J. Kindrachuk, R.F. Johnson, G.G. Olinger Jr., P.B. Jahrling, M. Laidlaw, L.M. Johansen, C.M. Lear-Rooney, P.J. Glass, L.E. Hensley, M.B. Frieman, Repurposing of clinically developed drugs for treatment of Middle East respiratory syndrome coronavirus infection, Antimicrob. Agents Chemother. 58 (2014) 4885–4893.

[70] R.A. Ali, C. Camick, K. Wiles, T.F. Walseth, J.T. Slama, S. Bhattacharya, D.R. Giovannucci, K.A. Wall, Nicotinic acid adenine dinucleotide phosphate plays a critical role in naive and effector murine t cells but not natural regulatory t cells, J. Biol. Chem. 291 (2016) 4503–4522.

[71] E. Lloyd-Evans, A.J. Morgan, X. He, D.A. Smith, E. Elliot-Smith, D.J. Sillence, G.C. Churchill, E.H. Schuchman, A. Galione, F.M. Platt, Niemann-Pick disease type C1 is a sphingosine storage disease that causes deregulation of lysosomal calcium, Nat. Med. 14 (2008) 1247–1255.

[72] D. Hoglinger, P. Haberkant, A. Aguilera-Romero, H. Riezman, F.D. Porter, F.M. Platt, A. Galione, C. Schultz, Intracellular sphingosine releases calcium from lysosomes, eLife 4 (2015).

[73] H. Belinson, D. Lev, E. Masliah, D.M. Michaelson, Activation of the amyloid cascade in apolipoprotein E4 transgenic mice induces lysosomal activation and neurodegeneration resulting in marked cognitive deficits, J. Neurosci. 28 (2008) 4690–4701.